

Supplemental material

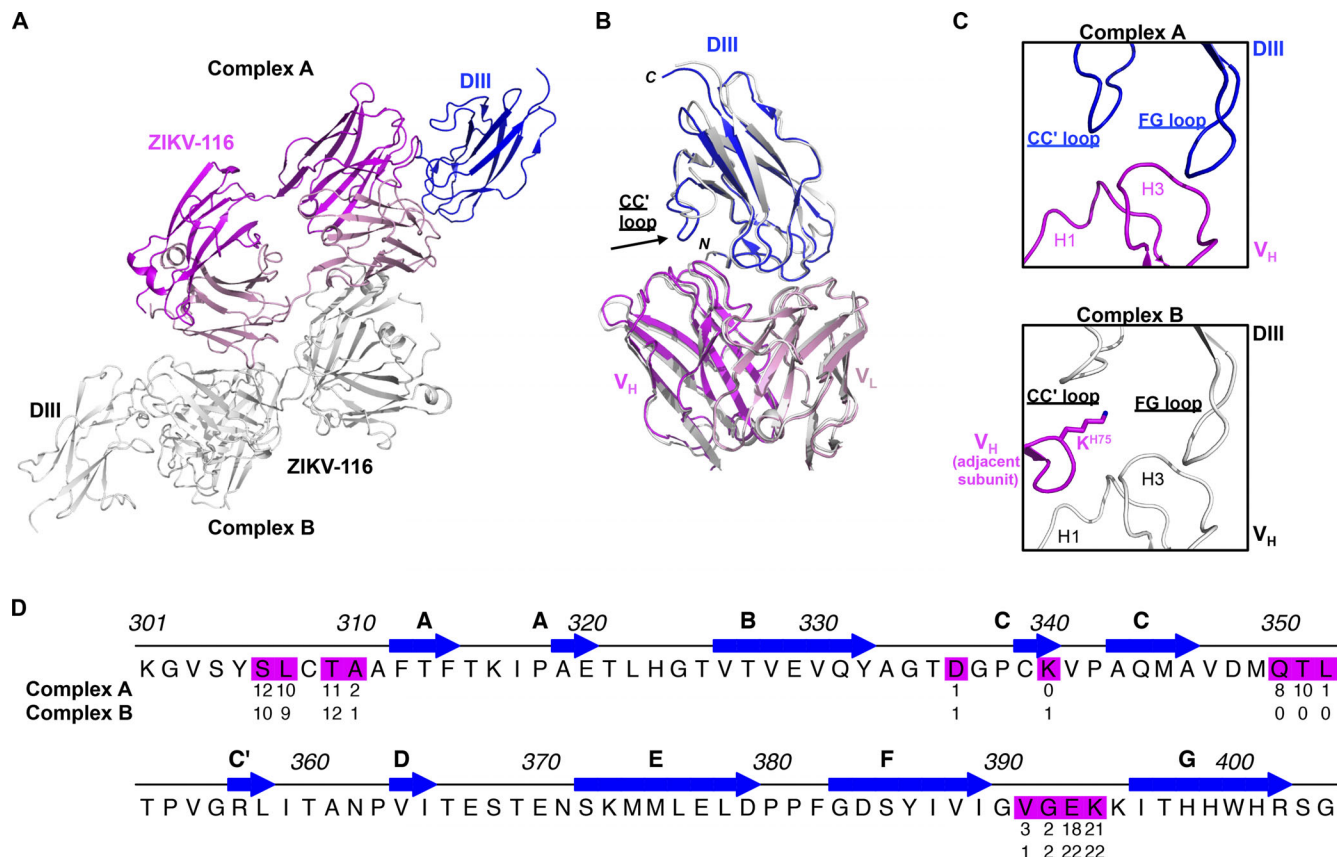
Zhao et al., <https://doi.org/10.1084/jem.20191792>

Figure S1. Asymmetric unit of the ZIKV-116-DIII complex. Related to Fig. 2. **(A)** There are two ZIKV-116-DIII complexes in one asymmetric unit of the crystal. Complex B is colored in white. In complex A, DIII is colored in blue, heavy chain in magenta, and light chain in pink. **(B)** Superimposition of DIII and variable domains of Fab between two ZIKV-116-DIII complexes. **(C)** Ribbon diagram of CC'-loop interface from complex A (upper) and complex B (down). Residue K^{H75} from adjacent asymmetric unit protruded into the ZIKV-116-DIII interface and interrupted the interaction between the CC'-loop of DIII and ZIKV-116 V_H in complex B. V_H from adjacent asymmetric unit is colored in magenta, and complex A and B are colored as above. **(D)** The DIII residues that make van der Waals contact distance <3.90 Å are colored, and the numbers below the ZIKV DIII represent the total number of contacts for each residue in each complex.

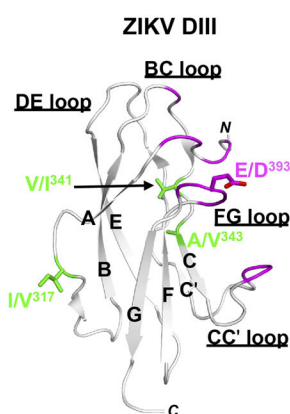
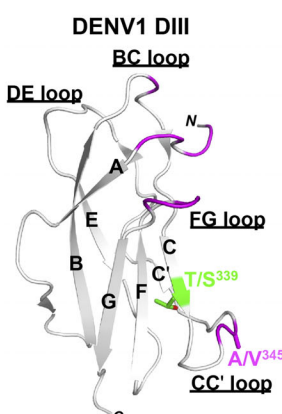
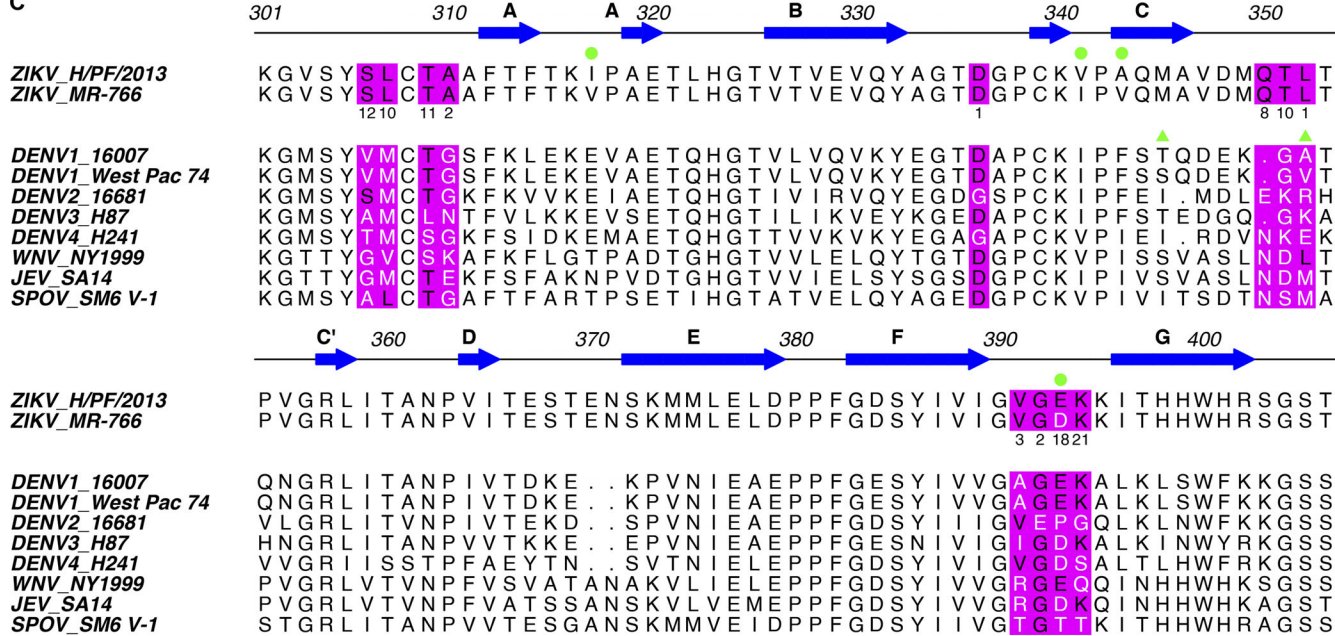
A**B****C**

Figure S2. Amino acid differences in DIII between ZIKV strains H/PF/2013 and MR-766, and DENV1 strains 16007 and West Pac-74. Related to Fig. 5. (A and B) Ribbon diagrams of ZIKV DIII (A) and DENV1 DIII (B). ZIKV-116 epitope residues are highlighted in magenta, and variable amino acids between two ZIKV strains or two DENV1 strains are indicated by sticks. (C) Sequence alignment of DIII from representative flaviviruses, and ZIKV-116 epitope residues are highlighted in magenta background. Conserved residues are shown in black text, and variable residues are shown in white text within the predicted ZIKV-116 epitope. Green circles mark amino acid variations between ZIKV H/PF/2013 and MR-766. Green triangles mark amino acid variations between DENV1 strains 16007 and West Pac-74.

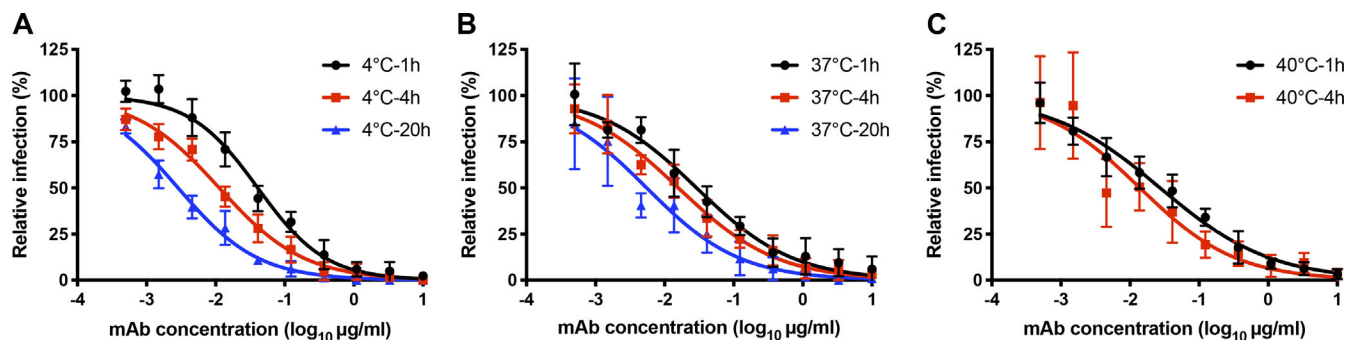


Figure S3. Time and temperature dependence of ZIKV inhibition. (A–C) ZIKV H/PF/2013 was incubated with ZIKV-116 or media for 1, 4, and 20 h at 4°C and 37°C (A and B) or 1 and 4 h at 40°C (C). Virus-mAbs or viruses alone were added to Vero cells after incubation, and infectivity was assessed 40 h later using an FFA assay. The relative infection was calculated by comparing no mAb-treated wells at each incubation time for each temperature. Data shown are pooled from two independent experiments in duplicate or triplicate. Error bars indicate SD.

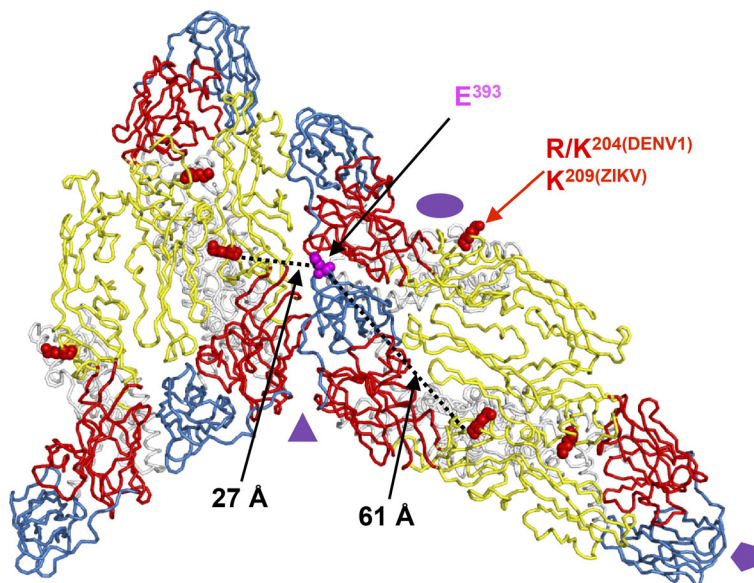


Figure S4. Residue 204^{DENV1}/209^{ZIKV} is located distally from the structural ZIKV-116 epitope. Two representative asymmetric units of the mature ZIKV virion (PDB 6CO8) are shown as ribbon structures (D1, red; DII, yellow; DIII, blue; transmembrane domain, white). The icosahedral symmetry axes are indicated by a purple oval (twofold), triangle (threefold), and pentagon (fivefold). Red spheres mark residue R/K^{204(DENV1)}/K^{209(ZIKV)}, and magenta spheres mark residue E³⁹³. The distance between the C_α of two residues are measured using PyMOL software. E³⁹³ is ~60 Å away from residue R/K^{204(DENV1)} on the E monomer, and the closest distance of E³⁹³ to R/K^{204(DENV1)} from adjacent E monomer is ~30 Å.

Table S1. Summary of crystallographic data

ZIKV-116-DIII	
Data collection	
Space group	P2 ₁
Cell dimensions	
<i>a, b, c</i> (Å)	72.81, 89.81, 92.49
<i>a, β, γ</i> (°)	90.00, 103.96, 90.00
Resolution (Å)	50–2.3 (2.34–2.30)
Total reflections	325,315
Unique reflections	50,077
Redundancy	6.5 (5.1)
Completeness (%)	97.5 (94.4)
<i>R</i> _{merge} (%)	9.8 (52.1)
<i>R</i> _{free} (%)	4.9 (25.5)
CC _{1/2}	1 (0.853)
<i>I</i> / <i>σI</i>	22.5 (2.8)
Wilson B-factor (Å ²)	42
Refinement	
Resolution (Å)	45–2.3 (2.34–2.30)
No. of reflections	50,016 (2,471)
<i>R</i> _{work} / <i>R</i> _{free} (%)	16.7/21.1 (25.6/29.4)
No. of atoms	
Protein	8,232
Water	407
<i>B</i> -factors	
DIII	49
Fab	44
Water	45
RMS deviations	
Bond lengths (Å)	0.004
Bond angles (°)	0.66
Ramachandran plot (%) ^a	97.67/2.33/0

*R*_{free} was calculated with 5% of the data. Numbers in parentheses represent values in the highest-resolution shell. RMS, root mean square.

^aResidues in favored, allowed, and disallowed regions of the Ramachandran plot.

Table S2. Van der Waals contacts for ZIKV-116-DIII complex

DIII (FIM) complex	ZIKV-116	DIII (EHL) complex	ZIKV-116
A		B	
Ser ^{E306}	Ser ^{H56} (5), Lys ^{H57} (3), Tyr ^{H58} (4)	Ser ^{E306}	Ser ^{H56} (6), Lys ^{H57} (2), Tyr ^{H58} (2)
Leu ^{E307}	Ser ^{H56} (3), Tyr ^{H58} (7)	Leu ^{E307}	Ser ^{H56} (2), Tyr ^{H58} (7)
Thr ^{E309}	Asp ^{L92} (1), Ser ^{L93} (3), Tyr ^{L94} (2), Trp ^{L96} (1), Tyr ^{H58} (3), Val ^{H100A} (1)	Thr ^{E309}	Asp ^{L92} (1), Ser ^{L93} (4), Tyr ^{L94} (3), Trp ^{L96} (1), Tyr ^{H58} (3)
Ala ^{E310}	Asp ^{L92} (2)	Ala ^{E310}	Asp ^{L92} (2), Ser ^{L93} (1)
Asp ^{E336}	Tyr ^{L94} (1)	Asp ^{E336}	Tyr ^{L94} (1)
		Lys ^{E340}	Asp ^{H55} (1)
Gln ^{E350}	Tyr ^{H32} (1), Ser ^{H98} (7)		
Thr ^{E351}	Asn ^{H31} (4), Arg ^{H99} (6)		
Leu ^{E352}	Arg ^{H99} (1)		
Val ^{E391}	Arg ^{H99} (2), Val ^{H100A} (1)	Val ^{E391}	Arg ^{H99} (1)
Gly ^{E392}	Glu ^{H100C} (2)	Gly ^{E392}	Glu ^{H100C} (2)
Glu ^{E393}	Arg ^{H96} (5), Leu ^{H97} (3), Glu ^{H100C} (7), Leu ^{H100D} (3)	Glu ^{E393}	Arg ^{H96} (7), Leu ^{H97} (2), Glu ^{H100C} (8), Leu ^{H100D} (4), Tyr ^{L91} (1)
Lys ^{E394}	Trp ^{L32} (11), Tyr ^{L91} (3), Asp ^{L92} (3), Glu ^{H100C} (4)	Lys ^{E394}	Trp ^{L32} (11), Tyr ^{L91} (3), Asp ^{L92} (4), Glu ^{H100C} (4)

The amino acids are superscripted to indicate their specific positions in the heavy chain (H), light chain (L), or DIII (E) sequences. Interactions were determined using the ligplot program with a cutoff distance of 3.90 Å. In complex A, the heavy chain is named as chain I, light chain is named as chain M, and DIII is named as chain F. In complex B, heavy chain is named as chain H, light chain is named as chain L, and DIII is named as chain E.

Table S3. Van der Waals contacts summary

	CDR-H1 (26–32)	CDR-H2 (52–56)	CDR-H3 (95–102)	FRM-H	Total V _H	CDR-L1 (24–34)	CDR-L3 (89–97)	Total V _L
FIM complex A	5	8	42	17	72	11	16	27
EHL complex B	0	9	28	14	51	11	21	32

Interactions were determined using the ligplot program with a cutoff distance of 3.90 Å.

Table S4. Direct hydrogen bond contacts

DIII (FIM, complex A)	ZIKV-116	DIII (EHL, complex B)	ZIKV-116
Ser ^{E306} (OG)	Lys ^{H57} (O)		
Leu ^{E307} (N)	Ser ^{H56} (OG), Tyr ^{H58} (OH)	Leu ^{E307} (N)	Ser ^{H56} (OG)
Leu ^{E307} (O)	Tyr ^{H58} (OH)	Leu ^{E307} (O)	Tyr ^{H58} (OH)
Thr ^{E309} (OG1)	Tyr ^{L94} (N)	Thr ^{E309} (OG1)	Tyr ^{L94} (N)
Gln ^{E350} (O)	Ser ^{H98} (OG)		
Glu ^{E393} (N)	Glu ^{H100C} (OE1)	Glu ^{E393} (N)	Glu ^{H100C} (OE1)
Glu ^{E393} (OE1)	Arg ^{H96} (NH1)	Glu ^{E393} (OE1)	Arg ^{H96} (NH1)
Glu ^{E393} (OE2)	Arg ^{H96} (NE)	Glu ^{E393} (OE2)	Arg ^{H96} (NE)
Lys ^{E394} (NZ)	Glu ^{H100C} (OE2), Tyr ^{L91} (O)	Lys ^{E394} (NZ)	Glu ^{H100C} (OE2), Tyr ^{L91} (O)

The amino acids are superscripted to indicate their specific positions in the heavy chain (H), light chain (L) or DIII (E) sequences. Interactions were determined using ligplot program with default setting.

Table S5. Indirect hydrogen bond contacts

DIII (FIM, complex A)	Water	ZIKV-116	DIII (EHL, complex B)	Water	ZIKV-116
Ser ^{E306} (OG)	S101	Lys ^{H57} (O)	Ser ^{E306} (OG)	S179	Lys ^{H57} (O)
Ala ^{E311} (N)	S97	Asp ^{L92} (O)	Ala ^{E311} (N)	S84	Asp ^{L92} (O)
Thr ^{E335} (OG1), Thr ^{E335} (N)	S341	Ser ^{L93} (OG)	Thr ^{E335} (OG1), Thr ^{E335} (N)	S18	Ser ^{L93} (OG)
Val ^{E391} (O), Lys ^{E394} (N)	S6	Glu ^{H100C} (OE2)	Val ^{E391} (O), Lys ^{E394} (N)	S10	Glu ^{H100C} (OE2)
Gly ^{E392} (N)	S108	Arg ^{H99} (O)	Gly ^{E392} (N)	S167	Arg ^{H99} (O)
Glu ^{E393} (OE1)	S15	Tyr ^{L91} (OH)	Glu ^{E393} (OE1)	S26	Tyr ^{L91} (OH)
Glu ^{E393} (OE2)	S59	<u>Asp^{H95}(OD1)</u> <u>Leu^{H97}(N)</u>	Glu ^{E393} (OE2)	S144	<u>Asp^{H95}(OD1)</u> <u>Leu^{H97}(N)</u>
			Ala ^{E333} (O)	S211	Asp ^{L92} (OD2)
Gln ^{E350} (NE2)	S156	Ser ^{H98} (OG, N)			
Gln ^{E350} (NE2)	S317	Asn ^{H31} (ND2)			
Gln ^{E350} (OE1)					

The amino acids are superscripted to indicate their specific positions in the heavy chain (H), light chain (L), or DIII (E) sequences. Interactions were determined using the ligplot program with default setting.

Table S6. Hydrogen bonds summary

	CDR-H1 (26-32)	CDR-H2 (52-56)	CDR-H3 (95-102)	FRM-H	Total V _H	CDR-L3 (89-97)	Total V _L
FIM, complex A	0+1	1+0	5+4	3+1	15	2+3	5
EHL, complex B	0+0	1+0	4+3	1+1	10	2+4	6

Hydrogen bond interactions (direct + indirect) were determined using the ligplot program with default setting.

Table S7. Neutralizing activity of ZIKV-116 and control mAb ZV-67 against different ZIKV strains

Strains	Genotype	Residue 393	ZIKV-116		ZV-67	
			IC ₅₀ (ng/ml)	IC ₉₀ (ng/ml)	IC ₅₀ (ng/ml)	IC ₉₀ (ng/ml)
H/PF/2013	Asian	E	27.4 ± 5.2	1,092 ± 396.5	236.1 ± 99.5	7,577 ± 3,558
Brazil Fortaleza	Asian	E	8.9 ± 2.6	136.7 ± 66.8	45.7 ± 4.9	1,511 ± 528.3
Cambodia FSS13025	Asian	E	19.3 ± 2.5	655.8 ± 114.3	146.4 ± 29.8	6,623 ± 715.4
Puerto Rico PRVABC58	Asian	E	8.2 ± 1.4	242.2 ± 44.0	74.6 ± 24.1	3,336 ± 877.7
Malaysia P6740	Asian	D	71.8 ± 10.8	8,435 ± 2,314	92.3 ± 15.7	4,027 ± 722.3
MR-766	African	D	365.1 ± 138.3	>100,000	104.1 ± 18.6	5,528 ± 2,824
Dakar 41519	African	D	246.9 ± 25.9	>40,000	301.9 ± 80.1	15,752 ± 5,431

The amount of mAbs that was required for 50% (IC₅₀) and 90% (IC₉₀) of inhibition is indicated. The indicated virus was incubated with serially diluted mAbs for 1 h at 37°C followed by addition of the mixture to Vero cells. Then, FRNT assays were performed, and the percentage of infection was calculated by comparing to no mAb-treated wells. ZIKV-116 shows greater neutralizing activity against most of ZIKV Asian strains than African strains. Control mAb ZV-67 neutralizes ZIKV Asian strains (H/PF/2013, Cambodia FSS13025, and Malaysia P6740) and African strains (MR-766 and Dakar 41519) with comparable IC₅₀. The results are the average of three or more independent experiments performed in duplicate or triplicate.

Table S8. BLI results for ZIKV and DENV1 DIII binding to mAbs

mAbs	DIII	Binding parameters ^a				
		k_a (10^5 M $^{-1}$ s $^{-1}$)	k_d (10 $^{-3}$ s $^{-1}$)	K_D (nM), kinetic	K_D (nM), equilibrium ^b	$t_{1/2}$ (min) ^c
ZIKV-116	DIII ^{H/PF/2013} (pH 5.5)	3.27 ± 0.29	0.73 ± 0.13	2.24 ± 0.19	5.05 ± 0.41	16.06 ± 2.62
ZIKV-116	DIII ^{H/PF/2013}	3.94 ± 0.14	0.45 ± 0.03	1.15 ± 0.07	7.54 ± 1.56	25.7 ± 1.84
ZIKV-116	DIII ^{MR-766}	3.91 ± 0.26	47.17 ± 6.40	121 ± 16.52	141 ± 22.34	0.25 ± 0.03
ZIKV-116	DIII ^{H/PF/2013} (E ^{393D})	3.76 ± 0.52	22.83 ± 5.28	62 ± 19.93	68.67 ± 9.32	0.52 ± 0.12
ZIKV-116	DIII ¹⁶⁰⁰⁷	1.84 ± 0.54	1.90 ± 0.08	10.7 ± 2.70	15.95 ± 6.72	6.10 ± 0.25
ZIKV-116	DIII ^{West Pac-74}	1.47 ± 0.41	1.86 ± 0.01	13.2 ± 3.82	16.75 ± 3.89	6.21 ± 0.04
ZIKV-116 V.J.Rev	DIII ^{H/PF/2013}	2.02 ± 0.20	9.82 ± 0.10	48.9 ± 5.37	68.15 ± 17.18	1.18 ± 0.01
ZIKV-116 V.J.Rev	DIII ^{MR-766}	0.65 ± 0.18	790.7 ± 194.6	12,233 ± 986.6	16,267 ± 2,479	0.015 ± 0.004
ZIKV-116 V.J.Rev	DIII ¹⁶⁰⁰⁷	0.34 ± 0.12	229.0 ± 9.90	7,160 ± 2,220	39,050 ± 34,578	0.05 ± 0.002
ZIKV-116 V.J.Rev	DIII ^{West Pac-74}	0.31 ± 0.09	199.5 ± 48.79	6,955 ± 3557	48,300 ± 41,861	0.065 ± 0.01

^aValues are means ± SD from at least two independent experiments.^b K_D , equilibrium was determined as described in the Materials and methods.^cCalculated from the dissociation constant: $t_{1/2} = \ln(2)/k_d$.

Table S9. Key resources

Reagent or resource	Source	Identifier
Antibodies		
Monoclonal anti-ZIKV-E ZIKV-116	This paper	N/A
Monoclonal anti-WNV-E E60	Michael S. Diamond, WUSTL, (mdiamond@wustl.edu)	Oliphant et al., 2006
Monoclonal anti-WNV-E E53	Michael S. Diamond, WUSTL	Oliphant et al., 2006
Monoclonal anti-WNV WNV-E111	Michael S. Diamond, WUSTL	Oliphant et al., 2006
Monoclonal anti-DENV1 DENV1-E111	Michael S. Diamond, WUSTL	Austin et al., 2012
Monoclonal anti-DENV4 DENV4-E88	Michael S. Diamond, WUSTL	Sukupolvi-Petty et al., 2013
Monoclonal anti-JEV JEV-106	Michael S. Diamond, WUSTL	Fernandez et al., 2018
Monoclonal anti-POWV POWV-61	This paper, unpublished mAb	N/A
Goat anti-human IgG-HRP	Santa Cruz Biotechnology	Cat# sc-2907
Goat anti-mouse IgG-HRP	Santa Cruz Biotechnology	Cat# sc-2005
Goat anti-mouse-PE	BD Pharmingen	Cat# 550589
Bacterial and virus strains		
ZIKV strain: French Polynesia_H/PF/2013	Michael S. Diamond, WUSTL	Zhao et al., 2016
ZIKV strain: Uganda_MR-766	Michael S. Diamond, WUSTL	Zhao et al., 2016
ZIKV strain: Senegal_Dakar 41519	Michael S. Diamond, WUSTL	Zhao et al., 2016
DENV1 strain 16007	Michael S. Diamond, WUSTL	Shrestha et al., 2010
DENV1 strain West Pac-74	Michael S. Diamond, WUSTL	Shrestha et al., 2010
BL21-CodonPlus-RIL competent cells	Agilent Technologies	Cat# 230240
Chemicals, peptides, and recombinant proteins		
EZ-Link-NHS-PEG4-Biotin	Thermo Fisher	Cat# 21330
Recombinant ZIKV-DIII from H/PF/2013	This paper	GenBank: AHZ13508.1
Recombinant ZIKV-DIII from MR-766	This paper	GenBank: ANO46296.1
Recombinant DENV1-DIII from 16007	Austin et al., 2012	N/A
Recombinant DENV1-DIII from West Pac-74	Austin et al., 2012	N/A
Recombinant DENV2-DIII	Austin et al., 2012	N/A
Recombinant DENV3-DIII	Austin et al., 2012	N/A
Recombinant DENV4-DIII	Austin et al., 2012	N/A
Recombinant WNV-DIII from New York 1999	Nybakken et al., 2005	N/A
Recombinant WNV-E from New York 1999	Luca et al., 2012	N/A
Recombinant JEV-DIII from SA14-14-2	Fernandez et al., 2018	N/A
Recombinant SPOV-E from SM6 V-1	This paper	GenBank: YP_009227187.1
Recombinant POWV-DIII from Spooner	This paper	GenBank: ADK37756.1
Critical commercial assays		
RNEasy Mini Purification Kit	Qiagen	Cat# 74104
SuperScript III First-Strand Synthesis System Thermo Fisher for RT-PCR	Thermo Fisher	Cat# 18080-051
4–12% Bis-Tris NuPAGE gel system	Thermo Fisher	Cat# 18080-051
FuGENE 6 Transfection Reagent		Cat# E2691
Deposited data		
ZIKV-116 Fab in complex with DIII structure	This paper	PDB: 6PLK
Experimental models: cell lines		
Vero	ATCC	Cat# CCL-81
Human: FreeStyle 293F	Thermo Fisher	Cat# R79007

Table S9. Key resources (Continued)

Reagent or resource	Source	Identifier
Human: FreeStyle 293F	Thermo Fisher	Cat# R79007
HEK 293T	ATCC	Cat# CRL-1573
Raji-DCSIGNR	Pierson laboratory	N/A
Recombinant DNA		
Plasmid: pML-huCG1	This paper	N/A
Plasmid: pET21a	This paper	N/A
Software and algorithms		
GraphPad Prism	GraphPad Software, Inc.	https://www.graphpad.com
FlowJo version 10	Tree Star	https://www.flowjo.com/solutions/flowjo/downloads
Biaevaluation 4.1	GE Healthcare	https://www.biacore.com/lifesciences/service/downloads/software_licenses/biaevaluation/
Phaser	McCoy et al., 2007	http://www ccp4.ac.uk/html/phaser.html
Phenix	Adams et al., 2010	https://www.phenix-online.org/
Coot	Emsley et al., 2010	https://www2.mrc-lmb.cam.ac.uk/personal/pemsley/coot/
PDBePISA	Open source	www.ebi.ac.uk/pdbe/pisa/
PyMOL	Schrödinger	https://www.pymol.org/
Ligplot	McDonald and Thornton, 1994	https://sbgrid.org/software/titles/ligplot
Agilent QuikChange Primer Design program	Agilent Technologies	N/A

N/A, not applicable; WUSTL, Washington University in St. Louis.

References

- Adams, P.D., P.V. Afonine, G. Bunkóczki, V.B. Chen, I.W. Davis, N. Echols, J.J. Headd, L.W. Hung, G.J. Kapral, R.W. Grosse-Kunstleve, et al. 2010. PHENIX: a comprehensive Python-based system for macromolecular structure solution. *Acta Crystallogr. D Biol. Crystallogr.* 66:213–221. <https://doi.org/10.1107/S0907444909052925>
- Austin, S.K., K.A. Dowd, B. Shrestha, C.A. Nelson, M.A. Edeling, S. Johnson, T.C. Pierson, M.S. Diamond, and D.H. Fremont. 2012. Structural basis of differential neutralization of DENV-1 genotypes by an antibody that recognizes a cryptic epitope. *PLoS Pathog.* 8:e1002930. <https://doi.org/10.1371/journal.ppat.1002930>
- Emsley, P., B. Lohkamp, W.G. Scott, and K. Cowtan. 2010. Features and development of Coot. *Acta Crystallogr. D Biol. Crystallogr.* 66:486–501. <https://doi.org/10.1107/S0907444910007493>
- Fernandez, E., N. Kose, M.A. Edeling, J. Adhikari, G. Sapparapu, S.M. Lazarte, C.A. Nelson, J. Govero, M.L. Gross, D.H. Fremont, et al. 2018. Mouse and human monoclonal antibodies protect against infection by multiple genotypes of Japanese encephalitis virus. *MBio.* 9:e00008-18. <https://doi.org/10.1128/mBio.00008-18>
- Luca, V.C., J. AbiMansour, C.A. Nelson, and D.H. Fremont. 2012. Crystal structure of the Japanese encephalitis virus envelope protein. *J. Virol.* 86:2337–2346. <https://doi.org/10.1128/JVI.06072-11>
- McCoy, A.J., R.W. Grosse-Kunstleve, P.D. Adams, M.D. Winn, L.C. Storoni, and R.J. Read. 2007. Phaser crystallographic software. *J. Appl. Cryst.* 40:658–674. <https://doi.org/10.1107/S0021889807021206>
- McDonald, I.K., and J.M. Thornton. 1994. Satisfying hydrogen bonding potential in proteins. *J. Mol. Biol.* 238:777–793. <https://doi.org/10.1006/jmbi.1994.1334>
- Nybakkene, G.E., T. Oliphant, S. Johnson, S. Burke, M.S. Diamond, and D.H. Fremont. 2005. Structural basis of West Nile virus neutralization by a therapeutic antibody. *Nature.* 437:764–769. <https://doi.org/10.1038/nature03956>
- Oliphant, T., G.E. Nybakken, M. Engle, Q. Xu, C.A. Nelson, S. Sukupolvi-Petty, A. Marri, B.-E. Lachmi, U. Olshevsky, D.H. Fremont, et al. 2006. Antibody recognition and neutralization determinants on domains I and II of West Nile Virus envelope protein. *J. Virol.* 80:12149–12159. <https://doi.org/10.1128/JVI.01732-06>
- Shrestha, B., J.D. Brien, S. Sukupolvi-Petty, S.K. Austin, M.A. Edeling, T. Kim, K.M. O'Brien, C.A. Nelson, S. Johnson, D.H. Fremont, and M.S. Diamond. 2010. The development of therapeutic antibodies that neutralize homologous and heterologous genotypes of dengue virus type 1. *PLoS Pathog.* 6:e1000823. <https://doi.org/10.1371/journal.ppat.1000823>
- Sukupolvi-Petty, S., J.D. Brien, S.K. Austin, B. Shrestha, S. Swayne, K. Kahle, B.J. Doranz, S. Johnson, T.C. Pierson, D.H. Fremont, and M.S. Diamond. 2013. Functional analysis of antibodies against dengue virus type 4 reveals strain-dependent epitope exposure that impacts neutralization and protection. *J. Virol.* 87:8826–8842. <https://doi.org/10.1128/JVI.01314-13>
- Zhao, H., E. Fernandez, K.A. Dowd, S.D. Speer, D.J. Platt, M.J. Gorman, J. Govero, C.A. Nelson, T.C. Pierson, M.S. Diamond, and D.H. Fremont. 2016. Structural basis of Zika virus-specific antibody protection. *Cell.* 166:1016–1027. <https://doi.org/10.1016/j.cell.2016.07.020>